

# Strongly polarized narrow exciton lines from $\text{Ga}_2\text{Se}_3/\text{GaSe}$ allotropic nanostructures

Maxim V. Rakhlin, Sergey V. Sorokin, Ilya A. Eliseyev, Valery Yu. Davydov,  
Demid A. Kirilenko, Alexey A. Toropov, and Tatiana V. Shubina\*

*Ioffe Institute, 194021 St. Petersburg, Russia*

E-mail: shubina@beam.ioffe.ru

## Abstract

The ability to emit narrow exciton lines, preferably with a well-defined polarization, is one of the key conditions for the use of nanostructures based on III-VI monochalcogenides in nanophotonics and quantum technologies (for single photon emitters). At present, the main method of their formation is the exfoliation of layered crystals, supplemented by strain and defect engineering. The factor limiting the use of epitaxy is the presence of different polytypes and structural phases in the grown films. However, control over their formation can make it possible to create structures with desired properties. In this work, we propose a  $\text{Ga}_2\text{Se}_3/\text{GaSe}$  nanostructure fabricated by van der Waals epitaxy with a high VI/III flux ratio as a source of strongly polarized narrow lines of exciton emission. In fact, this nanostructure is formed from allotropes: GaSe and  $\text{Ga}_2\text{Se}_3$ , which consist of the same atoms in different arrangements. The energy position of the narrow lines is determined by the quantum confinement in ultrathin  $\text{Ga}_2\text{Se}_3$  inclusions of different sizes in the GaSe matrix (barrier), and their linear polarization is due to the ordering of Ga vacancies in a certain crystal direction in  $\text{Ga}_2\text{Se}_3$ . Using transmission electron microscopy, Raman spectroscopy, and micro-photoluminescence,

the morphology of Ga<sub>2</sub>Se<sub>3</sub>/GaSe nanostructures, the temperature and temporal behavior of the narrow lines have been established. Our results open the way to the creation of allotropic nanostructures capable, in particular, of providing narrow-line emission.

## Introduction

The last decades can be characterized as an era of two-dimensional (2D) physics, when layered anisotropic semiconductors – transition metal dichalcogenides and group III metal monochalcogenides, studied since the middle of the last century, are being discovered from a new perspective. Monochalcogenides such as GaSe, GaS, and InSe are attracting much attention as parent materials for 2D and few-layer structures promising for applications in nanoelectronics (field-effect transistors), photovoltaics, sensors, and nonlinear optics.<sup>1–5</sup> Strain and defect engineering has been used to realize states in 2D structures, similar to quantum-dots, emitting narrow exciton lines and acting as sources of single photons.<sup>6</sup>

Gallium selenide is one of the most studied III–VI monochalcogenide semiconductors (see reviews<sup>7,8</sup>). Unlike transition metal dichalcogenides, bulk GaSe have almost degenerate indirect and direct band gaps, which greatly simplifies the problem of forming effectively emitting structures.<sup>9,10</sup> The published spectra of low-temperature photoluminescence (PL) of bulk GaSe are, as a rule, inhomogeneous and contain a series of lines that were attributed to free excitons and excitons bound at various defects.<sup>11</sup> The presence of different polytypes that differ from each other in the stacking sequence in the unit cell<sup>12–16</sup> can also contribute to the complexity of PL. As the number of monolayers decreases approximately to six, the emission from GaSe disappears due to very weak absorption of the exciting light in indirect gap structures.<sup>17</sup>

The so-called GaSe monolayer consists of four atomic layers, that is, a tetralayer, where two layers of Ga atoms are located between two layers of chalcogen atoms (Se-Ga-Ga-Se) (more details see in Supplementary). Such an architecture allows sliding of the Se sublayer, which leads to the appearance of intrinsic ferroelectricity.<sup>18</sup> In addition, the formation of an-

other structural phase,  $\text{Ga}_2\text{Se}_3$ , is possible. Essentially, it is an allotrope of  $\text{GaSe}$ , consisting of the same Ga and Se atoms, but in a different arrangement. It is the so-called defective zinc blende, which, in the case of the ordering of Ga vacancies, has either a monoclinic (mono) or orthorhombic (ortho) crystal structure (see Fig. S3 in Supplementary). The calculated band gap energy in mono- $\text{Ga}_2\text{Se}_3$  is somewhat higher than in ortho- $\text{Ga}_2\text{Se}_3$ .<sup>19,20</sup> The measured band gap values of  $\text{Ga}_2\text{Se}_3$  are characterized by a large scatter and depend both on the film preparation methods and on the spectroscopic technique used.<sup>21–25</sup> However, the difference in band gap between the mono- and ortho- phases is always within 0.5 eV and the mono-phase has a higher energy.

The ordered  $\text{Ga}_2\text{Se}_3$  has unique structural and electronic properties, which are almost independent on the particular crystal structure (mono or ortho), but rather on the vacancies and their local environment.<sup>26</sup> In contrast to  $\text{GaSe}$  ( $\text{Ga}_2\text{Se}_2$ ), one third of the gallium positions in this compound are not filled and represents structural vacancies. Such vacancies are located not randomly, but along every third line along a certain direction forming a “super-structure”, that is, an extended unit cell<sup>19</sup> (see Fig. S4 in Supplementary). As a result, the PL turns out to be strongly linearly polarized.<sup>22</sup> Similar phenomena, including optical anisotropy, were observed in  $\text{Ga}_2\text{S}_3$  as well.<sup>27</sup> The nanostructures of these materials have not yet been studied.

So far, chalcogenide nanostructures have been fabricated predominantly using exfoliation technology. However, this manual method does not provide reproducible quality and sizes of monolayers suitable for chip technology. A possible solution to the problem can be the use of epitaxial methods. Molecular beam epitaxy (MBE) has certain advantages over other technologies due to the use of high purity materials, ultrahigh vacuum in the chamber, as well as the possibility of implementing the layer thickness at the atomic level.<sup>28</sup> MBE in the van der Waals growth mode was proposed back in the 1990s<sup>29,30</sup> as a method for successful epitaxial growth even with a strong mismatch between the layer and substrate lattices ( $\Delta a/a$  up to 30% or more) and when their crystal structures are different. However, despite some

promising results,<sup>31-34</sup> van der Waals epitaxy of both mono- and dichalcogenides is still under development.<sup>35</sup>

In this paper, we report on the first successful formation of emitting Ga<sub>2</sub>Se<sub>3</sub>/GaSe nanostructures by the van der Waals MBE. The technology for their fabrication involves increasing the Se/Ga ratio by increasing the growth temperature. Raman studies and transmission electron microscopy (TEM) have shown that the grown samples contain ultrathin Ga<sub>2</sub>Se<sub>3</sub> inclusions. Using micro-PL spectroscopy ( $\mu$ -PL), highly linearly polarized narrow excitonic emission lines ( $\sim 1$  meV wide) are observed, as expected from the ordering of Ga vacancies in Ga<sub>2</sub>Se<sub>3</sub>. The short decay times ( $\sim 400$  ps) of the lines are consistent with the direct band gap of Ga<sub>2</sub>Se<sub>3</sub>, and their quenching with increasing temperature corresponds to the use of GaSe as a barrier.

## Sample growth and characterization

### Van der Waals epitaxy

Controlling the stoichiometry of van der Waals III-VI monochalcogenide films, tending to spontaneous formation of a large number of polytypes, requires a developed approach that takes into account relatively low growth temperatures as well as the possibility of the formation of transitional submonolayers at the heterointerface between the substrate and the layer.<sup>33,36,37</sup>

The sample under study was grown on a GaAs(001) substrate using a two-chamber MBE setup. First, a 200 nm thick GaAs buffer layer was grown in a separate III-V chamber, then transferred to the III-VI chamber through vacuum, and the growth of GaSe film was started at a substrate temperature of  $T_S=400^\circ\text{C}$ . Such a relatively low value of  $T_S$  provides the van der Waals growth mode with the orientation of the c axis of the growing GaSe layer perpendicular to the substrate surface, which ensures the formation of a sharp GaSe/GaAs(001) interface.<sup>33</sup> After the growth of the first  $\sim 4$  nm, the epitaxy temperature was raised to

$T_S \sim 500^\circ\text{C}$  and then remained unchanged until the end of the growth run. One of the main reasons for introducing this step is that GaSe layers grown at high  $T_S$  demonstrate efficient near band-edge PL in contrast to the films grown at low  $T_S$ .<sup>33</sup> On the other hand, higher  $T_S$  requires an increase in the VI/III ratio to avoid the appearance of Ga droplets on the growth surface. In this regard, it should be noted that the conditions established for the MBE growth of single-crystal Ga<sub>2</sub>Se<sub>3</sub> layers do not differ much from that for GaSe:  $T_S \sim 450\text{-}550^\circ\text{C}$  (i.e., nearly the same), VI/III ratio is 15 and higher (i.e., only a few times higher in contrast to GaSe) if both standard Ga and Se sources as well as GaP(001) or GaAs(001) substrates are used.<sup>38-41</sup> When using a valve cracking cell as a Se source, the VI/III ratio required to maintain conditions with the high Se content during GaSe growth is significantly higher and depends on the substrate temperature due to the lower selenium sticking coefficient. Such a high VI/III flux ratio, as well as relatively low growth temperatures ( $T_S \sim 500^\circ\text{C}$ ) can apparently promote the formation of a vacancy-ordered Ga<sub>2</sub>Se<sub>3</sub> phase inclusions in the growing film.<sup>20,40</sup> Proof of this assumption is the existence of a peak associated with Ga<sub>2</sub>Se<sub>3</sub> phase in the X-ray diffraction curves of GaSe layers grown at high VI/III flux ratio ( $\sim 30\text{-}40$ ) at  $T_S \sim 400^\circ\text{C}$  using a Se valve cracking cell (see Supplementary). Thus, one can expect the appearance of a small amount of Ga<sub>2</sub>Se<sub>3</sub> phase inclusions in GaSe layers grown in two-stage mode using the above parameters.

Scanning electron microscopy (SEM) cross-sectional images show that the total thickness of the grown film reached  $\sim 0.36 \mu\text{m}$  (Fig. 1)a. The film surface morphology is rough, enriched with trigonal or tetrahedral ridges, which results from the increase in temperature at the second stage. Further details of van der Waals epitaxy of GaSe can be found in the Methods section.

## Raman studies

GaSe crystals consisting of Ga-Se-Se-Ga tetralayers exist as  $\beta$ ,  $\gamma$ ,  $\delta$ , and  $\epsilon$ <sup>42-44</sup> polytypes, which differ in mutual arrangement of tetralayers in a unit cell. To determine the main

polytype of the sample grown by van der Waals epitaxy, we carried out Raman studies in a wide frequency range. The  $\epsilon$  polytype occurs most frequently in epitaxial thin films. Within the framework of the  $D_{3h}$   $\epsilon$ -GaSe symmetry group nomenclature, the high-frequency ( $\omega > 50 \text{ cm}^{-1}$ ) Raman spectra of bulk GaSe contain lines 60, 134, 214, 252 and  $308 \text{ cm}^{-1}$  corresponding to  $E''$ ,  $A_1^1$ ,  $E'(TO)$ ,  $E'(LO)$  and  $A_1'$  respectively.<sup>45,46</sup> As seen in Figure 1b, the Raman spectrum measured in the grown sample contains all these high-frequency lines. In addition, modes in the low-frequency region ( $\omega < 50 \text{ cm}^{-1}$ ) make it possible to accurately determine the polytype.<sup>46</sup> Here we observe one peak at  $19 \text{ cm}^{-1}$ , which convincingly confirms the predominance of the  $\epsilon$  polytype of GaSe in the studied thin film.

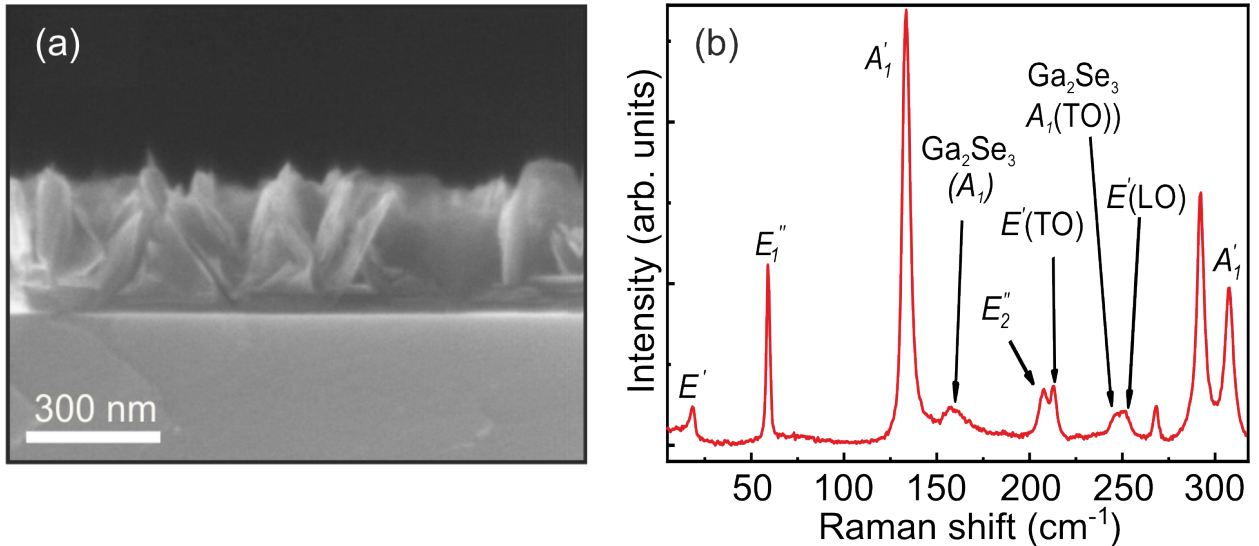


Figure 1: SEM image of the cross section (a) and unpolarized Raman spectrum (b) of a GaSe sample grown by van der Waals MBE on GaAs (001).

The vacancy-ordered  $\text{Ga}_2\text{Se}_3$  can exist in both monoclinic and orthorhombic modifications, whose electronic properties are similar.<sup>26</sup> We denote these modifications as “mono” and “ortho”, although some studies used the designations  $\beta\text{-Ga}_2\text{Se}_3$  for mono and  $\gamma\text{-Ga}_2\text{Se}_3$  for ortho.<sup>47</sup> In the Raman spectrum of the sample under study, the  $155 \text{ cm}^{-1}$  and  $\sim 250 \text{ cm}^{-1}$  modes are observed, which were previously registered in  $\text{Ga}_2\text{Se}_3$ .<sup>48-50</sup> The peak at  $155 \text{ cm}^{-1}$  can be attributed to the  $A_1$  mode of the vacancy-ordered phase.<sup>48</sup> The broadened shape of the peak indicates a change in the crystallinity of the  $\text{Ga}_2\text{Se}_3$  inclusions; a similar shape was

observed in<sup>50</sup> for specimens grown at relatively low VI/III flux ratios. In the region of 250  $\text{cm}^{-1}$ , a doublet is observed, consisting of two peaks: a weak  $E'(LO)$  peak of bulk GaSe (252  $\text{cm}^{-1}$ ) and a peak at 245  $\text{cm}^{-1}$ . It was suggested that the latter may be due to short-range interactions in the  $\text{Ga}_2\text{Se}_3$  unit cell.<sup>51</sup> Thus, the Raman spectrum is a combination of modes at frequencies characteristic of  $\epsilon$ -GaSe and vacancy-ordered  $\text{Ga}_2\text{Se}_3$ .

In addition, several lines in the Raman spectrum in Figure 1b arise from growth on the GaAs substrate and ridge morphology. For example, two additional lines at 268 and 291  $\text{cm}^{-1}$  correspond to transverse (TO) and longitudinal (LO) optical phonons of the GaAs substrate. A distinct doublet at 200-220  $\text{cm}^{-1}$  is a sign of rough morphology,<sup>33</sup> when the appearance of the low-frequency  $E_2''$  mode in GaSe became possible due to the inclination of the ridge face depending on the incident light.<sup>45,52</sup> Oxidation of GaSe in air can lead to the release of selenium<sup>53</sup> and the appearance of weak of the  $\text{Ga}_2\text{O}_3$  modes.<sup>54</sup>

## Transmission electron microscopy

The coexistence of the allotropic  $\epsilon$ -GaSe and  $\text{Ga}_2\text{Se}_3$  phases in the MBE-grown sample was confirmed by TEM studies of a thin flake (ridge) mechanically separated from the substrate (Fig. 2) shows both the  $\epsilon$ -GaSe hexagonal phase with a period of 0.8 nm and the  $\text{Ga}_2\text{Se}_3$  phase with a period of  $\sim 0.6$  nm at the top of this flake. These phases, conjugated by their close-packed planes, have a small mismatch of about 2%. The  $\text{Ga}_2\text{Se}_3$  inclusions have, on average, a thickness of several monolayers and a transverse size of about 5 nm. In addition, hexagonal  $\epsilon$ -GaSe has a fairly high stacking-fault density, which is clearly seen from electron diffraction (not shown here).

According to previous theoretical studies,<sup>19,55</sup> only two types of short-range ordering of vacancies are possible in  $\text{Ga}_2\text{Se}_3$ , which can occur either along  $[\bar{1}10]$  in ortho- $\text{Ga}_2\text{Se}_3$  or a zigzag line along  $[1\bar{1}2]$  to mono- $\text{Ga}_2\text{S}_3$ ,<sup>19</sup> although some uncertainty in the possible directions is still exists. In a orthorhombic cell  $a = 5.477 \text{ \AA}$ ,  $c = 5.414 \text{ \AA}$ , while in a monoclinic structure  $a = 6.66 \text{ \AA}$ ,  $c = 11.65 \text{ \AA}$ , i.e. the value of  $c$  is twice as large.<sup>20</sup> Therefore, in this flake we are

most likely observing ortho-Ga<sub>2</sub>Se<sub>3</sub>. Note that such characterization using TEM is possible only at the thin tip of the trigonal flake, since the thicker part near the substrate is opaque for this method.

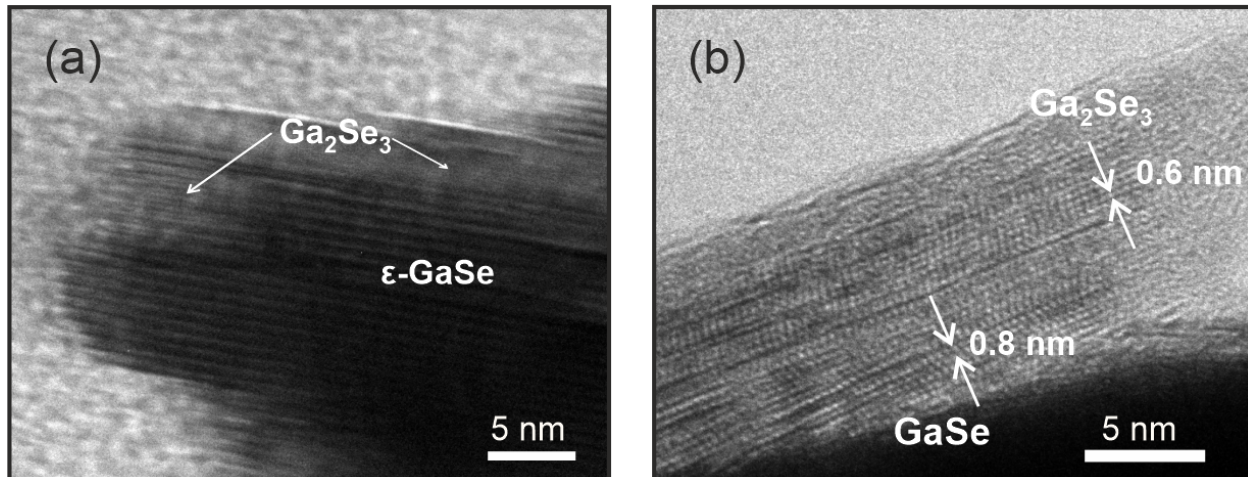


Figure 2: High-resolution TEM images of Ga<sub>2</sub>Se<sub>3</sub>/GaSe nanostructures in cross-sectional geometry: (a) general view with Ga<sub>2</sub>Se<sub>3</sub> insertions within GaSe; (b) enlarged image of the region with the Ga<sub>2</sub>Se<sub>3</sub> phase.

However, in this part, the stresses caused by the mismatch between the lattice parameters of the layer and the substrate are stronger, which can stimulate the formation of a monoclinic phase with a zigzag arrangement of vacancies, which is structurally more stable.<sup>20</sup> Thus, the formation of both ortho- and mono-Ga<sub>2</sub>Se<sub>3</sub> in the film under study cannot be ruled out.

## Narrow exciton lines

The possibility of quantum confinement in Ga<sub>2</sub>Se<sub>3</sub> inclusions depends on their characteristic dimensions relative to the exciton Bohr radius  $R_B$ . In the first approximation, we can assume that it is close to  $R_B = 4.5$  nm in bulk GaSe.<sup>56</sup> In this case, the exciton diameter of 9 nm significantly exceeds the characteristic sizes of Ga<sub>2</sub>Se<sub>3</sub> inclusions determined by the TEM method, and quantum confinement can provide the formation of distinct exciton levels, as in quantum dots. Therefore, the corresponding radiation must have a narrow radiation line width and a higher energy than the bulk material. The minimum energy of direct band

gap transitions in bulk ortho-Ga<sub>2</sub>Se<sub>3</sub> is about 1.75-1.85 eV.<sup>19</sup> Although published data are strongly dispersed for mono-Ga<sub>2</sub>Se<sub>3</sub>, it is reliably established that its band gap is noticeably higher.

The emission spectra measured in a grown film with a spatial resolution of  $\sim 1 \mu\text{m}$  at low temperature (10 K) and low excitation power (0.2 mW) demonstrate ultra-narrow lines (Fig. 3). It should be emphasized that such narrow lines are registered in local places. With a slight shift, narrow lines quickly disappear (see Supplementary). The ultra-narrow lines have a width of about 1 meV. Their intensity and number are increased as the excitation spot is defocused up to several  $\mu\text{m}$ . During laser defocusing, the direction of the incident light deviates slightly from the normal to the substrate, which is obviously preferable for the effective excitation of Ga<sub>2</sub>Se<sub>3</sub> inclusions located inside inclined flakes (see the excitation diagram in Fig. 3). Under this condition, a weak peak at 2.12 eV corresponding to GaSe emission is also resolved. The region where ultranarrow lines appear (1.85-2.08 eV) indicates a possible combination of ortho (in the lower part) and mono (in the upper part) Ga<sub>2</sub>Se<sub>3</sub> inclusions, for which the surrounding GaSe is a barrier.

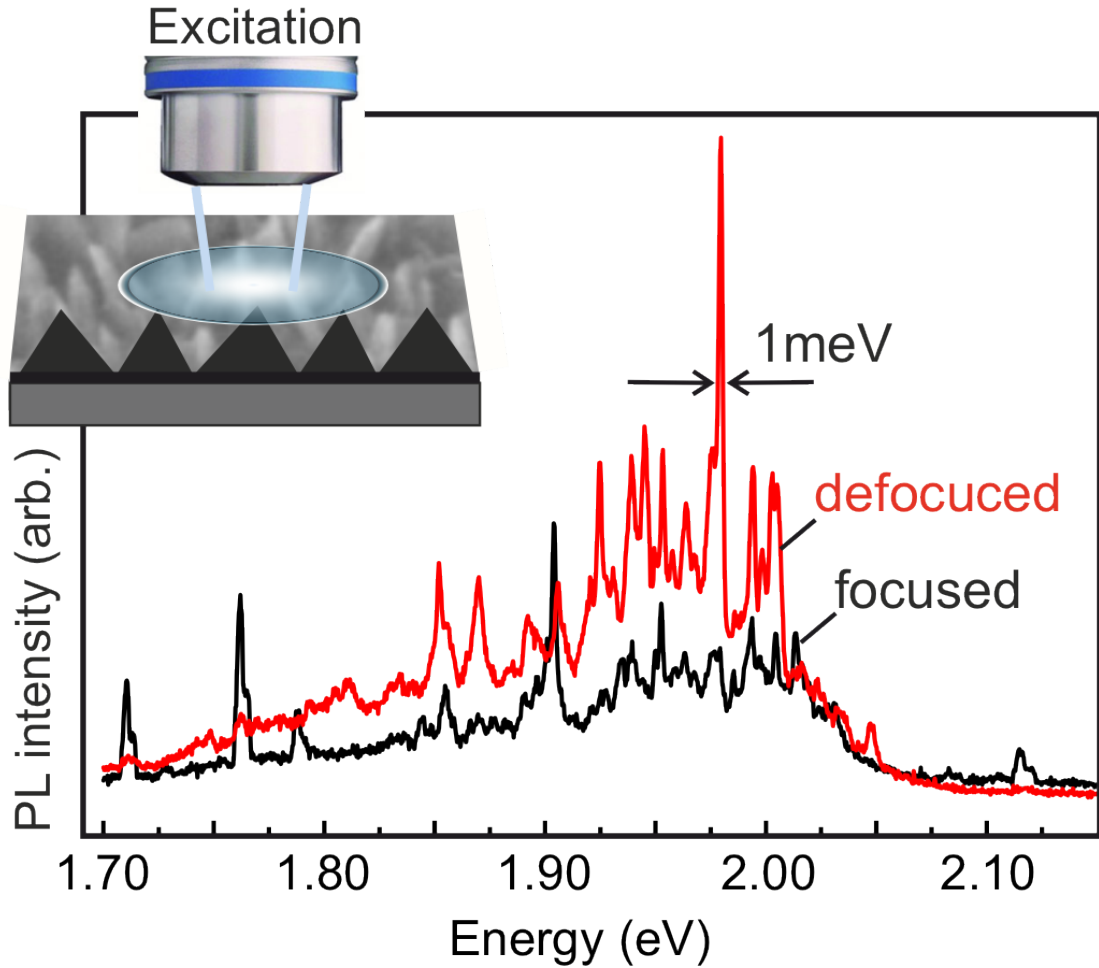


Figure 3: Narrow-line PL spectra recorded in a  $\text{Ga}_2\text{Se}_3/\text{GaSe}$  film with different excitation spot (focused to  $1\ \mu\text{m}$  and defocused). The excitation is illustrated by the inset against the bird-view SEM. Excitation power 0.2 mW, temperature 10 K.

At a higher excitation power (1 mW), a broad band appears centered around 1.73 eV (Fig. 4). This band is modulated by different peaks with a width of  $\sim 3\ \text{meV}$ . These peaks are probably due to the localization of excitons on structural defects, such as stacking faults, which were diagnosed by TEM in the film under study. Previously, we observed similar peaks in micro-PL spectra measured directly at stacking faults crossing ZnSe quantum wells.<sup>57</sup> Such peaks and ultranarrow lines behave differently with increasing temperature: ultranarrow lines disappear first in the upper region of the spectrum, since the GaSe barrier is not too high for  $\text{Ga}_2\text{Se}_3$  inclusions, and broader peaks localized at deeper defect centers still exist. Interestingly, in bulk GaSe, the free exciton peak dominates in the PL spectra at elevated

temperatures, although defect lines are present (see inset in Fig. 4).

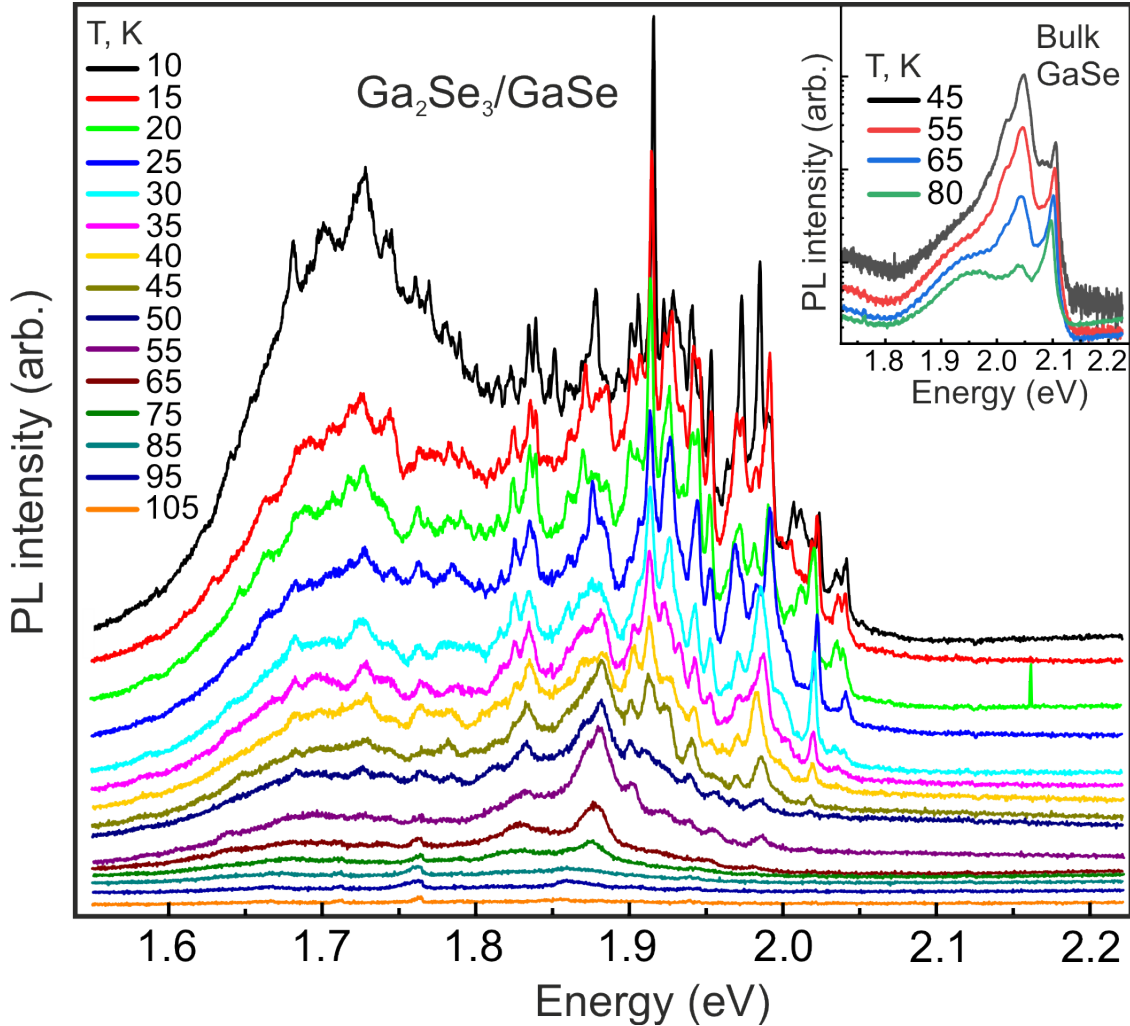


Figure 4: Narrow-line PL spectra recorded at various temperatures in Ga<sub>2</sub>Se<sub>3</sub>/GaSe. For comparison, the inset shows the PL spectra in bulk GaSe, where the exciton peak begins to dominate with increasing temperature.

An important argument in favor of the correctness of our interpretation of ultranarrow lines can be their linear polarization. The large linear anisotropy of the transmission spectra in a vacancy-ordered bulk Ga<sub>2</sub>Se<sub>3</sub> was first discovered in 1994 by Okamoto et al.<sup>22</sup> Later this phenomenon was theoretically considered by Nakayama and Ishikawa<sup>19</sup> and Péressy et al.<sup>26</sup> It is shown that optical transitions in Ga<sub>2</sub>Se<sub>3</sub> must be strictly linearly polarized along certain crystal directions, where vacancies form a one-dimensional super-structure. The ordering of vacancies occurs along a line in the  $[\bar{1}10]$  direction in ortho-Ga<sub>2</sub>Se<sub>3</sub> and in the form of a zigzag

along  $[1\bar{1}2]$  in mono-Ga<sub>2</sub>Se<sub>3</sub>. With a more complex zigzag ordering, optical anisotropy may appear due to the off-diagonal component of the dielectric function tensor, which changes the main axis of the crystal towards the direction of vacancy ordering.<sup>19</sup> As a result, a large optical anisotropy should be observed in measurements along and perpendicular to the corresponding direction in both mono- and ortho-Ga<sub>2</sub>Se<sub>3</sub>, and without a shift in the PL line energy.

We have performed micro-PL polarization measurements within the full planar angle from  $-180^\circ$  to  $+180^\circ$ , which confirm our findings. A simultaneous change in the polarization of narrow lines in Figure 5a indicates a strictly oriented crystallographic direction of the radiating objects located inside the excited spot. The difference in the angles of reaching the maximum and minimum of the PL intensity,  $I$ , is exactly  $90^\circ$ , as shown in Fig. 5c. The degree of polarization, defined as  $(I_\perp - I_\parallel)/(I_\perp + I_\parallel)$ , varies from  $\sim 40\%$  to  $60\%$  for different narrow lines. We emphasize that such anisotropy is demonstrated by an ensemble of separate Ga<sub>2</sub>Se<sub>3</sub>/GaSe nanostructures, whereas earlier the phenomenon was studied in bulk Ga<sub>2</sub>Se<sub>3</sub>.<sup>22,25,41</sup>

At some points, it turns out to be possible to register simultaneously two sets of lines, the polarization angle of which is shifted with relative to each other by  $60^\circ$ - $90^\circ$  (Fig. 5 (b,d)). In one of the set, the lines of the strongest intensity are concentrated near 1.9 eV, and in the other, near 2.0 eV. Accordingly, we attribute these sets to the radiation of the orthorhombic and monoclinic Ga<sub>2</sub>Se<sub>3</sub> phases, which have the corresponding band gap energy for the bulk  $\sim 1.75$  eV and  $\sim 1.9$  eV. The higher-energy lines arise from mono-Ga<sub>2</sub>Se<sub>3</sub> inclusions located closer to the substrate, where the stresses caused by the lattice misfit is stronger. The shift between the angles of polarization maxima in these two sets is due to the different crystal axes of the vacancy ordering in these two modifications of the defective zinc blende structure. Thus, this is an important observation that confirms the existence of two structural phases of Ga<sub>2</sub>Se<sub>3</sub>/GaSe nanostructures implemented in the sample under study.

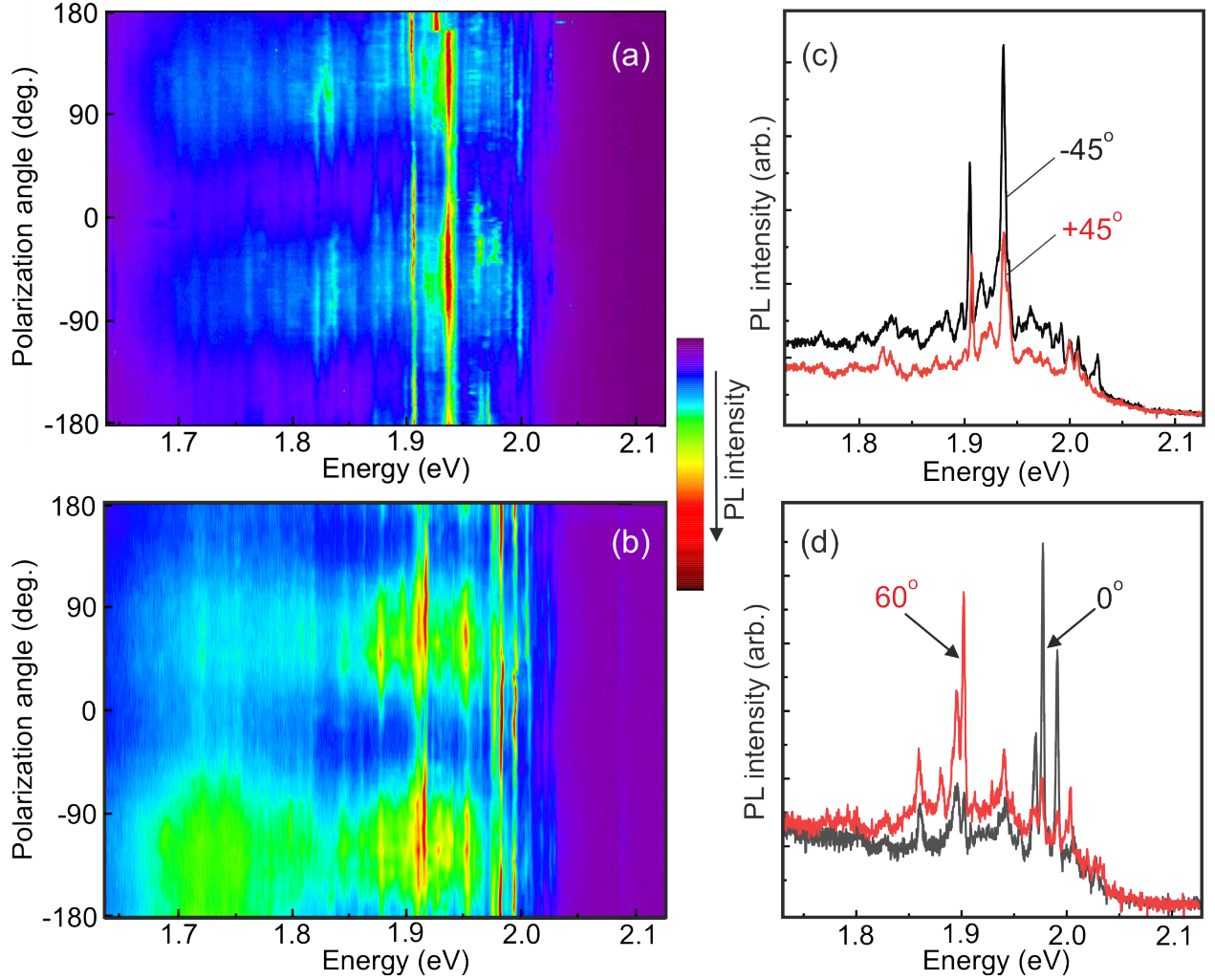


Figure 5: (a, b) Mapping of the polarized spectra of narrow PL lines measured over the full planar angle from  $-180^\circ$  to  $+180^\circ$  in two characteristic points demonstrating the dominance of the ortho phase (a) and the combination of the ortho and mono phases (b). The selected spectra demonstrate: (c) a difference of  $90^\circ$  between the angles of maximum and minimum intensity in the ortho phase; (d) shows the spectra characteristic of the ortho and mono phases.

Finally, we studied the type of optical transitions (direct or indirect) corresponding to the narrow lines. Previously, by measuring the absorption and cw PL, it was shown that bulk  $\text{Ga}_2\text{Se}_3$  has a direct band gap.<sup>21,27,47</sup> We assume that the measurements of time-resolved  $\mu$ -PL (TRPL) at low temperature is also one of the reliable methods, since in the case of a direct band structure the characteristic decay times should be much shorter than those of an indirect one. Figure 6 shows the measured decay curves of the ultra-narrow lines

possessing different wavelengths. The 629-nm (1.97 eV) line probably comes from mono-Ga<sub>2</sub>Se<sub>3</sub>, and the following lines with wavelengths of 650 nm or more come from ortho-Ga<sub>2</sub>Se<sub>3</sub>. The characteristic decay times of the dominant component in all narrow lines are about 400 ps. Such short decay times are characteristic of direct-gap transitions. They cannot be attributed to GaSe, where indirect transitions dominate at low temperatures and have much longer decay times, on the order of tens of nanoseconds. For reference, we present in Supplementary the data on the PL decay in bulk GaSe. The presence of a weak and slowly decaying component in the decay curves is due to the admixture of radiation from the surrounding GaSe. We cannot prevent this, since the detection area of 1  $\mu\text{m}$  significantly exceeds the dimensions of the Ga<sub>2</sub>Se<sub>3</sub>/GaSe nanostructures. However, at a lower excitation power (0.1 mW), when only the covering GaSe layer is effectively excited, the fast component from the inserts disappears.

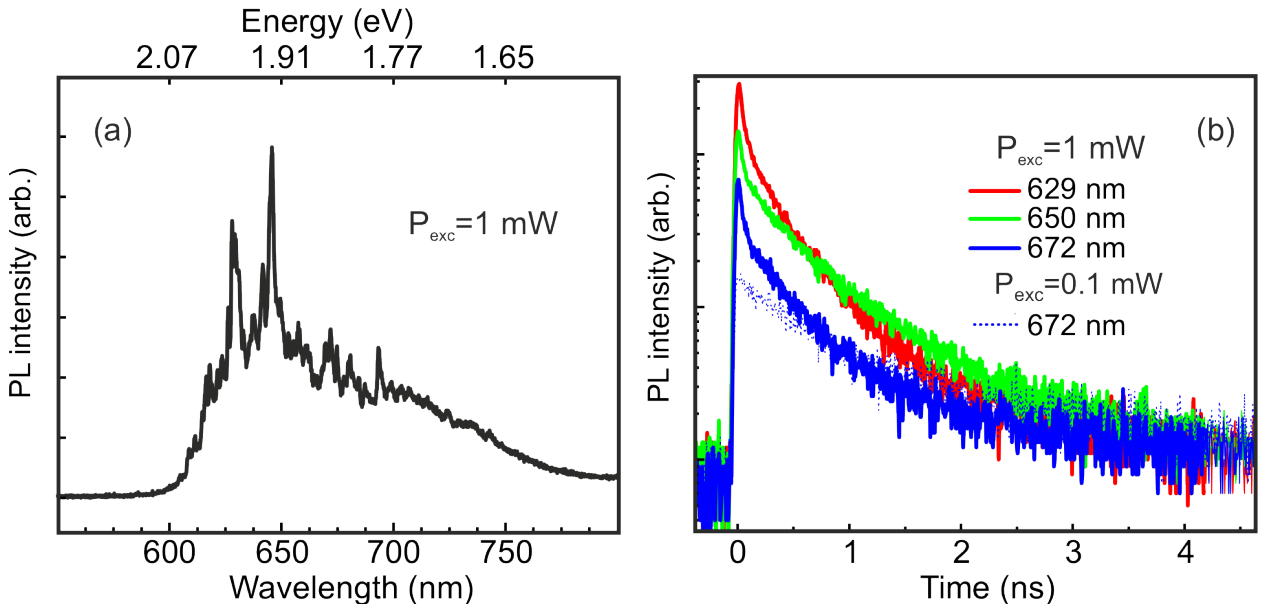


Figure 6: (a) Narrow-line PL spectrum and (b) PL decay curves of selected narrow lines measured at the indicated wavelengths at 10 K using a 405-nm pulsed-laser line. The excitation power is shown in the graphs.

Thus, these Ga<sub>2</sub>Se<sub>3</sub>/GaSe nanostructures have a direct type of transitions with a corresponding alignment of the conduction and valence bands, which is very important for the device application of the narrow lines.

## Conclusions

Summarizing, this work presents Ga<sub>2</sub>Se<sub>3</sub>/GaSe nanostructures grown by van der Waals epitaxy. The specificity of these nanostructures is that they can hardly be called "hetero" structures, since they are formed from related materials, consisting of the same atoms, but having different crystal structures. At a certain extent, they are allotropic compounds. These nanostructures demonstrate ultra-narrow lines of exciton radiation with a linewidth of  $\sim 1$  meV. The presence of the narrow lines in the emission spectra is possible as long as the energy of their quantum levels does not exceed the height of the potential barrier, which is the surrounding GaSe matrix. Importantly, the lines are strongly polarized with the degree of polarization up to 60%. Taking into account the energy position of the narrow lines and their polarization, we assumed that the lines are associated with excitons confined in the Ga<sub>2</sub>Se<sub>3</sub> inclusions which have the vacancy-ordered orthorhombic or monoclinic crystal structure. The existence of both crystal phases is confirmed by the pattern of polarized PL mapping, in which the emission maxima of high-energy and low-energy sets of narrow lines are shifted by a certain angle relative each other. The time-resolved micro-PL spectroscopy established the direct-gap nature of Ga<sub>2</sub>Se<sub>3</sub>/GaSe nanostructures. This combination of optical properties is unique for monochalcogenide nanostructures. A similar ordering of vacancies is possible in Ga<sub>2</sub>S<sub>3</sub> and, possibly, in other monochalcogenides such as In<sub>2</sub>Se<sub>3</sub> and In<sub>2</sub>Te<sub>3</sub>, which paves the way for the use of allotropic nanostructures in quantum photonics.

## Experimental section

### Van der Waals epitaxy

A (Ga,Se)-based layer was grown on epi-ready GaAs(001) substrate using a two-chamber MBE setup (SemiTEq production). A standard Ga cell and Se valve cracking cell (Veeco, USA) with the cracking zone temperature  $T_{Se(cr)}=500^\circ\text{C}$  were used as molecular beam

sources. To avoid problems with thermal cleaning of the substrate to remove the native oxide layers in the absence of an As flux, a GaAs buffer layer 200 nm thick was grown in a separate III-V chamber and then transferred to the III-VI chamber through vacuum. When the substrate temperature was stabilized at a targeted value of  $T_S=400^\circ\text{C}$ , the growth of GaSe was initiated with simultaneous opening the Ga and Se shutters. After the growth of first  $\sim 4$  nm, the epitaxy temperature was increased up to the  $T_S\sim 500^\circ\text{C}$ . The VI/III flux ratio was controlled by measuring the beam equivalent pressures (BEPs) of the corresponding elements at the substrate position by using a Bayard-Alpert ion gauge and maintained as high as  $\sim 20$  and  $\sim 30$  for the  $T_S=400^\circ\text{C}$  and  $500^\circ\text{C}$ , respectively. Taking into account that the stoichiometric conditions on the growth surface correspond to  $P_{Se}/P_{Ga} \sim 12$  and  $\sim 25$  at these growth temperatures,<sup>33</sup> the actual VI/III flux ratio can be estimated as  $\sim 1.2$  and  $1.6$  for the first and second stages of growth, respectively.

## Structural characterization

SEM characterization was performed using JEOL JSM 7001F scanning electron microscope. The crystal structure of mechanically separated flakes was investigated by TEM studies using a Jeol JEM-2100F microscope.

## Micro-Raman measurements

Raman spectra were obtained in backscattering geometry at room temperature. For these investigations, we used a Horiba LabRAM HREvo UV-VIS-NIR-Open spectrometer (Horiba, Lille, France) with confocal optics. Olympus MPLN100x (Olympus, Tokyo, Japan) objective lens (NA = 0.9) focused the laser beam in a spot  $\sim 1 \mu\text{m}$  in diameter. As an excitation source, a Nd:YAG laser (Torus Laser Quantum, Stockport, UK) with  $\lambda = 532 \text{ nm}$  was used. To avoid damage and heating of the sample, the laser power on its surface was limited to  $80 \mu\text{W}$ . A set of Bragg reflection and transmission filters was used to obtain Raman spectra in ultra-low-frequency range ( $\omega < 50 \text{ cm}^{-1}$ ).

## Micro-photoluminescence measurements

$\mu$ -PL setup was used for optical properties investigation of GaSe structures. Non resonant optical excitation of a *cw* laser (405 nm) was used for the  $\mu$ -PL measurements. Incident radiation was focused in 2-3  $\mu\text{m}$  spot on the sample by an apochromatic objective lens with NA of 0.42. The power density was  $\sim 4 \text{ W/cm}^2$ . The collected emission was dispersed by a 0.5m monochromator with a 600/mm grating for detection  $\mu$  PL spectra at selected wavelengths. For time-resolved  $\mu$ -PL studies the 405 nm line of a pulsed laser was used. Polarization control was achieved by means of a halfwave plate and a film polarizer installed in the detection channel.

## Conflict of Interest

The authors declare no conflict of interest.

## Author Contributions

The manuscript was written using contributions of all authors. In particular, M.V.R. and I.A.E. contributed to  $\mu$ -PL and Raman studies, respectively. S.V.S. contributed to MBE growth. D.A.K. contributed to TEM measurements. V.Yu.D., A.A.T. and T.V.S. proposed a general physical model and supervised this work. All authors have given approval to the final version of the manuscript.

## Acknowledgement

The work of M.V.R. and I.A.E. was supported by a grant from the Russian Science Foundation (no. 22-22-20049, <https://rscf.ru/project/22-22-20049/>) and a grant from the St. Petersburg Science Foundation in accordance with agreement no. 21/2022 dated April 14, 2022.

## Supporting Information Available

The data that support the findings of this study are available in the supplementary material of this article.

## References

- (1) Bourdon, A.; Bringuier, E.; Portella, M.; Vivières, M.; Piccioli, N. Angular properties of second-harmonic polarization due to high-order nonlinearities: Application to GaSe and InSe. *Physical Review Letters* **1990**, *65*, 1925.
- (2) Guo, J.; Xie, J.-J.; Li, D.-J.; Yang, G.-L.; Chen, F.; Wang, C.-R.; Zhang, L.-M.; Andreev, Y. M.; Kokh, K.; Lanskii, G.; Svetlichnyi, V. Doped GaSe crystals for laser frequency conversion. *Light: Science & Applications* **2015**, *4*, e362.
- (3) Sato, Y.; Tang, C.; Watanabe, K.; Ohsaki, J.; Yamamoto, T.; Tanabe, T.; Oyama, Y.  $\text{In}_x\text{Ga}_{1-x}\text{Se}$  mixed crystals grown from an In flux by the traveling heater method for THz wave generation. *Journal of Physics Communications* **2020**, *4*, 1065007.
- (4) Cai, H.; Gu, Y.; Lin, Y.-C.; Yu, Y.; Geohegan, D.; Xiao, K. Synthesis and emerging properties of 2D layered III–VI metal chalcogenides. *Applied Physics Reviews* **2019**, *6*, 041312.
- (5) Wang, Y.; Gao, J.; Wei, B.; Han, Y.; Wang, C.; Gao, Y.; Liu, H.; Han, L.; Zhang, Y. Reduction of the ambient effect in multilayer InSe transistors and a strategy toward stable 2D-based optoelectronic applications. *Nanoscale* **2020**, *12*, 18356–18362.
- (6) Tonndorf, P.; Schwarz, S.; Kern, J.; Niehues, I.; Pozo-Zamudio, O. D.; Dmitriev, A. I.; Bakhtinov, A. P.; Borisenko, D. N.; Kolesnikov, N. N.; Tartakovskii, A. I.; de Vasconcelos, S. M.; Bratschitsch, R. Single-photon emitters in GaSe. *2D Materials* **2017**, *4*, 021010.

- (7) Belen'kii, G. L.; Stopachinskii, V. B. Electronic and vibrational spectra of III-VI layered semiconductors. *Soviet Physics Uspekhi* **1983**, *26*, 497–517.
- (8) Sarkar, A. S.; Stratakis, E. Recent Advances in 2D Metal Monochalcogenides. *Advanced Science* **2020**, *7*, 2001655.
- (9) Sun, Y.; Luo, S.; Zhao, X.-G.; Biswas, K.; Li, S.-L.; Zhang, L. InSe: a two-dimensional material with strong interlayer coupling. *Nanoscale* **2018**, *10*, 7991–7998.
- (10) Lai, K.; Ju, S.; Zhu, H.; Wang, H.; Wu, H.; Yang, B.; Zhang, E.; Yang, M.; Li, F.; Cui, S.; Deng, X.; Han, Z.; Zhu, M.; Dai, J. Strong bulk-surface interaction dominated in-plane anisotropy of electronic structure in GaTe. *Communications Physics* **2022**, *5*, 143.
- (11) Capozzi, V.; Montagna, M. Optical spectroscopy of extrinsic recombinations in gallium selenide. *Physical Review B* **1989**, *40*, 3182.
- (12) Brebner, J. L.; Mooser, E. Excitons in GaSe polytypes. *Physics Letters A* **1967**, *24*, 274–275.
- (13) Blasi, C. D.; Manno, D.; Rizzo, A. Convergent-beam electron diffraction study of melt- and vapour-grown single crystals of gallium chalcogenides. *Il Nuovo Cimento D* **1989**, *11*, 1145–1163.
- (14) Ueno, K.; Takeda, N.; Sasaki, K.; Koma, A. Investigation of the growth mechanism of layered semiconductor GaSe. *Applied Surface Science* **1997**, *113*, 38–42.
- (15) Dai, Z.; Chegwidan, S. R.; Rumaner, L. E.; Ohuchi, F. S. Microstructure evolution of GaSe thin films grown on GaAs(100) by molecular beam epitaxy. *Journal of Applied Physics* **1999**, *85*, 2603–2608.
- (16) Liu, S.; Yuan, X.; Wang, P.; Chen, Z.-G.; Tang, L.; Zhang, E.; Zhang, C.; Liu, Y.; Wang, W.; Liu, C.; Chen, C.; Zou, J.; Hu, W.; Xiu, F. Controllable Growth of Vertical

- Heterostructure GaTe<sub>x</sub>Se<sub>1-x</sub>/Si by Molecular Beam Epitaxy. *ACS Nano* **2015**, *9*, 8592–8598.
- (17) Pozo-Zamudio, O. D.; Schwarz, S.; Sich, M.; Akimov, I. A.; Bayer, M.; Schofield, R.; Chekhovich, A.; Robinson, B. J.; Kay, N.; Kolosov, O. V.; Dmitriev, A. I.; Lashkarev, G.; Borisenko, D. N.; Kolesnikov, N. N.; Tartakovskii, A. I. Photoluminescence of two-dimensional GaTe and GaSe films. *2D Materials* **2015**, *2*, 035010.
- (18) Li, W.; Zhang, X.; Yang, J.; Zhou, S.; Song, C.; Cheng, P.; Zhang, Y.-Q.; Feng, B.; Wang, Z.; Lu, Y.; Wu, K.; Chen, L. Emergence of ferroelectricity in a nonferroelectric monolayer. *Nature Communications* **2023**, *14*, 2757.
- (19) Nakayama, T.; Ishikawa, M. Bonding and Optical Anisotropy of Vacancy-Ordered Ga<sub>2</sub>Se<sub>3</sub>. *Journal of the Physical Society of Japan* **1997**, *66*, 3887–3892.
- (20) Huang, G.-Y.; Abdul-Jabbar, N.; Wirth, B. First-principles study of the structure and band structure of Ga<sub>2</sub>Se<sub>3</sub>. *Journal of Physics: Condensed Matter* **2013**, *25*, 225503.
- (21) Park, K.-H.; Kim, H.-G.; Kim, W.-T.; Kim, C.-D.; Jeong, H.-M.; Lee, K.-J.; Lee, B.-H. Optical properties of Ga<sub>2</sub>Se<sub>3</sub>:Co<sup>2+</sup> single crystals. *Solid State Communications* **1989**, *70*, 971–974.
- (22) Okamoto, T.; Yamada, A.; Konagai, M.; Takahashi, K. Polarized photoluminescence in vacancy-ordered Ga<sub>2</sub>Se<sub>3</sub>. *Journal of Crystal Growth* **1994**, *138*, 204–207.
- (23) Morley, S.; von der Emde, M.; Zahn, D. R. T.; Offermann, V.; Ng, T. L.; Maung, N.; Wright, A. C.; Fan, G. H.; Poole, I. B.; Williams, J. O. Optical spectroscopy of epitaxial Ga<sub>2</sub>Se<sub>3</sub> layers from the far infrared to the ultraviolet. *Journal of Applied Physics* **1996**, *79*, 3196–3199.
- (24) von der Emde, M.; Zahn, D.; Ng, T.; Maung, N.; Fan, G.; Poole, I.; Williams, J.;

- Wright, A. MOCVD growth of Ga<sub>2</sub>Se<sub>3</sub> on GaAs(100) and GaP(100): a Raman study. *Applied Surface Science* **1996**, *104-105*, 575–579.
- (25) Lovejoy, T.; Yitamben, E.; Ohta, T.; Fain, S.; Ohuchi, F.; Olmstead, M. One-dimensional electronic states in Ga<sub>2</sub>Se<sub>3</sub> on Si(001):As. *Physical Review B* **2010**, *81*, 245313.
- (26) Peressi, M.; Baldereschi, A. Structural and electronic properties of Ga<sub>2</sub>Se<sub>3</sub>. *Journal of Applied Physics* **1998**, *83*, 3092–3095.
- (27) Ho, C.-H.; Chen, H.-H. Optically decomposed near-band-edge structure and excitonic transitions in Ga<sub>2</sub>S<sub>3</sub>. *Scientific Reports* **2014**, *4*, 6143.
- (28) Toropov, A.; Evropeitsev, E.; Nestoklon, M.; Smirnov, D.; Shubina, T.; Kaibyshev, V.; Budkin, G.; Jmerik, V.; Nechaev, D.; Rouvimov, S.; Ivanov, S.; Gil, B. Strongly Confined Excitons in GaN/AlN Nanostructures with Atomically Thin GaN Layers for Efficient Light Emission in Deep-Ultraviolet. *Nano Letters* **2020**, *20*, 158–165.
- (29) Ohuchi, F.; Parkinson, B.; Ueno, K.; Koma, A. van der Waals epitaxial growth and characterization of MoSe<sub>2</sub> thin films on SnS<sub>2</sub>. *Journal of Applied Physics* **1990**, *68*, 2168–2175.
- (30) Koma, A. van der Waals epitaxy for highly lattice-mismatched systems. *Journal of Crystal Growth* **1999**, *201*, 236–241.
- (31) Yuan, X.; Tang, L.; Wang, P.; Chen, Z.; Zou, Y.; Su, X.; Zhang, C.; Liu, Y.; Wang, W.; Liu, C.; Chen, F.; Zou, J.; Zhou, P.; Hu, W.; Xiu, F. Wafer-scale arrayed p-n junctions based on few-layer epitaxial GaTe. *Nano Research* **2015**, *8*, 3332.
- (32) Sorokin, S.; Avdienko, P.; I.V. Sedova, D. K.; Yagovkina, M.; Smirnov, A.; Davydov, V.; Ivanov, S. Molecular-Beam Epitaxy of Two-Dimensional GaSe Layers on GaAs(001) and

- GaAs(112) Substrates: Structural and Optical Properties. *Semiconductors* **2019**, *53*, 1131–1137.
- (33) Sorokin, S. V.; Avdienko, P.; Sedova, I.; Kirilenko, D.; Davydov, V.; Komkov, O.; D.D. Firsov, D.; Ivanov, S. Molecular Beam Epitaxy of Layered Group III Metal Chalcogenides on GaAs(001) Substrates. *Materials* **2020**, *13*, 3447.
- (34) Ohtake, A.; Sakuma, Y. Two-dimensional WSe<sub>2</sub>/MoSe<sub>2</sub> heterostructures grown by molecular-beam epitaxy. *The Journal of Physical Chemistry C* **2021**, *125*, 11257–11261.
- (35) Singh, D. K.; Gupta, G. van der Waals epitaxy of transition metal dichalcogenides via molecular beam epitaxy: looking back and moving forward. *Materials Advances* **2022**, *3*, 6142–6156.
- (36) Komkov, O.; Khakhulin, S.; Firsov, D.; Avdienko, P.; Sedova, I.; Sorokin, S. Investigation of Built-in Electric Fields at the GaSe/GaAs Interface by Photoreflectance Spectroscopy. *Semiconductors* **2020**, *54*, 1198–1204.
- (37) Dai, Z.; Ohuchi, F. Vacancy ordering of Ga<sub>2</sub>Se<sub>3</sub> at GaSe/GaAs(100) interface. *Applied Physics Letters* **1998**, *73*, 966–968.
- (38) Teraguchi, N.; Konagai, M.; Kato, F.; Takahashi, K. Growth and characterization of Ga<sub>2</sub>Se<sub>3</sub> by molecular beam epitaxy. *Journal of Crystal Growth* **1991**, *115*, 798–801.
- (39) Teraguchi, N.; Kato, F.; Konagai, M.; Takahashi, K.; Nakamura, Y.; Otuska, N. Vacancy ordering of Ga<sub>2</sub>Se<sub>3</sub> films by molecular beam epitaxy. *Applied Physics Letters* **1991**, *59*, 567–569.
- (40) Okamoto, T.; Takegami, T.; Yamada, A.; Konagai, M. Control of the Arrangement of the Native Gallium Vacancies in Ga<sub>2</sub>Se<sub>3</sub> on (100)GaAs by Molecular Beam Epitaxy. *Japanese Journal of Applied Physics* **1995**, *34*, 5984–5988.

- (41) Okamoto, T.; Konagai, M.; Kojima, N.; Yamada, A.; Takahashi, K.; Nakamura, Y.; Nittono, O. Anomalous anisotropy in the absorption coefficient of vacancy-ordered Ga<sub>2</sub>Se<sub>3</sub>. *Journal of Electronic Materials* **1993**, *22*, 229–232.
- (42) Nagel, S.; Baldereschi, A.; Maschke, K. Tight-binding study of the electronic states in GaSe polytypes. *Journal of Physics C: Solid State Physics* **1979**, *12*, 1625.
- (43) Schlüter, M. The Electronic Structure of GaSe. *Il Nuovo Cimento* **1973**, *3*, 313.
- (44) Segura, A. Layered Indium Selenide under High Pressure: a Review. *Crystals* **2018**, *8*, 206.
- (45) Hoff, R. M. Raman scattering in GaSe. *The Journal of Physical Chemistry C* **1975**, *53*, 17.
- (46) Lei, S.; Ge, L.; Liu, Z.; Najmaei, S.; Shi, G.; You, G.; Lou, J.; Vajtai, R.; Ajayan, P. Synthesis and Photoresponse of Large GaSe Atomic Layers. *Nano Letters* **2013**, *13*, 2777–2781.
- (47) Ho, C.-H. Ga<sub>2</sub>Se<sub>3</sub> defect semiconductors: the study of direct band edge and optical properties. *ACS Omega* **2020**, *5*, 18527–18534.
- (48) Finkman, E.; Tauc, J.; Kershaw, R.; Wold, A. Lattice dynamics of tetrahedrally bonded semiconductors containing ordered vacant sites. *Physical Review B* **1975**, *11*, 3785.
- (49) Kolodziejczyk, M.; Filz, T.; Krost, A.; Richter, W.; Zahn, D. The likelihood of III–2–VI<sub>3</sub> compound formation during epitaxial growth of II–VI on III–V semiconductors. *Journal of Crystal Growth* **92**, *117*, 549—553.
- (50) Yamada, A.; Kojima, N.; Takanashi, R. Raman study of epitaxial Ga<sub>2</sub>Se<sub>3</sub> films grown by molecular beam epitaxy. *Japanese Journal of Applied Physics* **1992**, *31*, L186.

- (51) von der Emde, M.; Zahn, D.; Ng, T.; Maung, N.; Fan, G.; Poole, I.; Williams, J.; Wright, A. MOCVD growth of Ga<sub>2</sub>Se<sub>3</sub> on GaAs(100) and GaP(100): a Raman study. *Applied Surface Science* **1995**, *104/105*, 575–579.
- (52) Irwin, J.; Hoff, R.; Clayman, B.; Bromley, R. Long wavelength lattice vibrations in GaS and GaSe. *Solid State Communications* **1973**, *13*, 1531–1536.
- (53) Beechem, T.; Kowalski, B.; Brumbach, M.; McDonald, A.; Spataru, C.; Howell, S.; Ohta, T.; Pask, J.; Kalugin, N. Oxidation of ultrathin GaSe. *Applied Physics Letters* **2015**, *107*, 173103.
- (54) Susoma, J.; Lahtinen, J.; Kim, M.; Riikonen, J.; Lipsan, H. Crystal quality of two-dimensional gallium telluride and gallium selenide using Raman fingerprint. *AIP Advances* **2017**, *7*, 015014.
- (55) Newman, P. Crystal structures of adamantane compounds. *Journal of Physics and Chemistry of Solids* **1962**, *23*, 19.
- (56) Budweg, A.; Yadav, D.; Grupp, A.; Leitenstorfer, A.; Trushin, M.; Pauly, F.; Brida, D. Control of excitonic absorption by thickness variation in few-layer GaSe. *Physical Review B* **2019**, *100*, 045404.
- (57) Smirnov, D.; Belyaev, K.; Kirilenko, D.; Nestoklon, M. O.; Rakhlin, M. V.; Toropov, A.; Sedova, I.; Sorokin, S.; Ivanov, S.; Gil, B.; Shubina, T. Exciton Bound to 1D Intersections of Stacking Fault Planes with a ZnSe Quantum Well. *Physica Status Solidi-Rapid Research Letters* **2018**, *12*, 1700410.